International Conference on the Physics of Reactors "Nuclear Power: A Sustainable Resource"
Casino-Kursaal Conference Center, Interlaken, Switzerland, September 14-19, 2008

Three-dimensional depletion analysis of the axial end of a Takahama fuel rod

Mark D. DeHart[a, *], Ian C. Gauld[a], Kenya Suyama[b]

[a] *Oak Ridge National Laboratory, Oak Ridge, Tennessee, USA*
[b] *Japan Atomic Energy Agency, Tokai-mura, Ibaraki-ken, Japan*

Abstract

Recent developments in spent fuel characterization methods have involved the development of several three-dimensional depletion algorithms based on Monte Carlo methods for the transport solution. However, most validation done to-date has been based on radiochemical assay data for spent fuel samples selected from locations in fuel assemblies that can be easily analyzed using two-dimensional depletion methods. The development of a validation problem that has a truly three-dimensional nature is desirable to thoroughly test the full capabilities of advanced three-dimensional depletion tools. This paper reports on the results of three-dimensional depletion calculations performed using the T6-DEPL depletion sequence of the SCALE 5.1 code system, which couples the KENO-VI Monte Carlo transport solver with the ORIGEN-S depletion and decay code. Analyses are performed for a spent fuel sample that was extracted from within the last two centimeters of the fuel pellet stack. Although a three-dimensional behavior is clearly seen in the results of a number of calculations performed under different assumptions, the uncertainties associated with the position of the sample and its local surroundings render this sample of little value as a validation data point.

1. Introduction

The dynamics of reactor operation result in non-uniform axial-burnup profiles in fuel with any significant burnup. At the beginning of life in a pressurized water reactor (PWR), given the near-cosine axial-shaped flux, the fuel near the axial center of a fuel assembly will be depleted at a greater rate than at the assembly ends. As the reactor continues to operate, the cosine flux shape will flatten because of the fuel depletion and fission product buildup that occurs near the center. However, because of the high leakage near the end of the fuel, burnup will drop off rapidly near the ends. Partial-length absorbers or non-uniform axial fuel loadings can further complicate the burnup profile. In a boiling-water reactor (BWR), the same phenomena come into play, but the burnup profile is complicated by the significant axial variation of moderator density and by non-uniform axial loadings of burnable poison rods.

Burnup Credit, a criticality safety analysis philosophy that takes partial credit for the burnup of fuel in away-from-reactor storage configuration, must take into account the axial variation in burnup in order to be conservative in the prediction of

[*] Corresponding author, DeHartMD@ornl.gov
Tel. +865-576-3468; Fax +865-574-9619.

reactivity of spent fuel (DeHart, 1996). In a reactor core, the axial flux profile is driven primarily by fresh to low-burnup fuel and has a flattened cosine profile; however, a criticality event in a cask or pool loaded with spent fuel will be driven by the low burnup ends of the loaded fuel assemblies, with fission peaks near the ends the fuel.

Numerous studies of axial burnup effects have been published (Brady et al, 1990, Turner, 1989, DeHart, 1996, 1999, Nouri, 1988, Wagner and DeHart, 2000). However, most analyses performed in estimation of isotopic distributions due to axial burnup profiles have been based on a set of two-dimensional (2-D) calculations performed for discrete burnup values that would represent the axial burnup distribution in a fuel assembly. In general, this approach works quite well, as the in-core axial gradient of the neutron flux is small over most of the length of the fuel rod, and the 2-D approximation is appropriate.

Conversely, because the axial gradient becomes significant as one approaches either end of the fuel assembly, the 2-D approximation begins to break down. This is further compounded by the axial neutron reflection of primarily thermal neutrons. It has been rationalized that axial leakage will lead to a reduced fast flux relative to the thermal flux, softening the spectrum near the ends of the fuel, and that a 2-D approximation is conservative in that it provides more plutonium production. This has not been put to the test, however, for two reasons – lack of good three-dimensional (3-D) analysis methods acceptable for away-from-reactor applications, and, more importantly, a scarcity of experimental measurements for fuel taken from the end regions of a fuel rod.

A number of 3-D depletion approaches based on Monte Carlo methods have been introduced within the last decade, including but not limited to TRITON (DeHart and Bowman, 2005), MONTEBURNS (Poston and Trellue, 1999), SWAT2 (Mochizuki et al., 2003), and ALEPH (Haeck, 2007); a full listing would be quite extensive. Verification and validation of these methods have primarily relied on available radiochemical assay (RCA) data. RCA measurements provide a quantative measurement (albeit with experimental uncertainties) of isotopic concentrations for select isotopes extracted from spent fuel samples.

Recent measurements on fuel from two discharged assemblies of the Takahama Unit 3 PWR provide data for fuel samples taken from locations very close to the top of the active region of the fuel rod. Results of TRITON-based 3-D depletion calculations completed in the analysis of the Takahama fuel sample are discussed in this paper.

2. Approach

The T6-DEPL sequence of the TRITON module in SCALE 5.1 (DeHart and Bowman, 2005) was used for isotopic calculations. TRITON is a SCALE control module that enables depletion calculations to be performed by coordinating iterative calls the CENTRM/PMC cross-section processing codes, a transport solver, and the ORIGEN-S point-depletion code. In the T6-DEPL sequence, KENO-VI is used as the transport solver, is applied to calculate weighted burnup-dependent cross sections that are employed to update ORIGEN-S libraries and to provide localized fluxes used for multiple depletion regions. TRITON uses a predictor-corrector approach to perform fuel-assembly burnup calculations.

Depletion calculations were performed based on the depletion history provided for fuel sample SF97-1 (Nakahara et al., 2000). This sample, located at an estimated height of 0.4cm from the top of the fuel rod (active region), was burned to an estimated 17.69 GWd/MTU. Several approaches were taken to develop a representative model of the spent fuel sample and it's environment, as described in the following subsections.

2.1. Base assembly model

A top-half assembly KENO-VI model was developed using reflection at the axial midplane of the assembly; Figure 1 illustrates the assembly configuration. Sample SF97-1 was located on the assembly periphery, as indicated by the green fuel positions in the model. The sample was place in each of four symmetric positions to improve statistics.

Isotopic concentrations were individually tracked for the sample rod with remaining fuel rods modelled as a group. All fuel rod models were divided into 15 axial segments, with the seven top segments having a height of 0.9cm each, based on the fuel pellet size; a finite sample size is required to collect sufficient neutron histories for reasonable statistics in the Monte Carlo simulation. The assembly model also included ten burnable poison

rods, each represented with four equal-volume rings to properly capture burnup effects; fuel rods were modelled using a single radial zone.

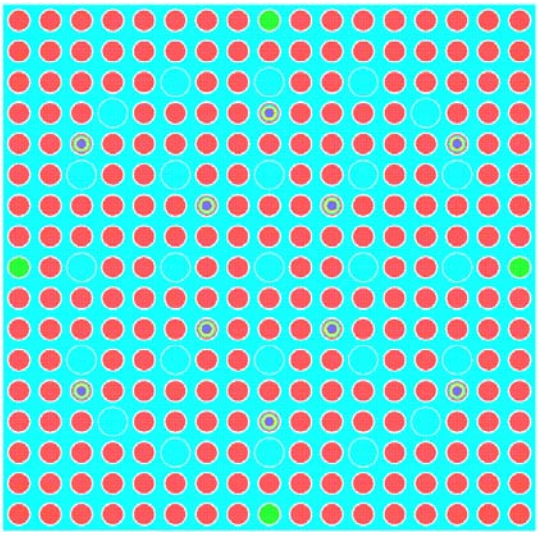

Fig. 1. Two-dimensional planar representation of Takahama fuel assembly model, with sample location shown in green.

Calculations were performed with 10,000 generations of 1000 neutrons each, with the first 1000 generations skipped. The cross section library used was the SCALE ENDF/B-VI 238-group energy structure. Weighted multigroup cross sections were calculated using point data and the CENTRM transport solver for resolved resonance energies.

Local moderator temperature and density reported for the pellet location were assumed for the entire length of the assembly. The impact of this assumption was felt to be trivial for PWR moderator; full axial data were not available.

2.2. Depletion model

The SF97-1 fuel sample was depleted to a total burnup of 17.69 GWd/MTU (determined based on neodymium measurements) during three cycles of operation, with cycle lengths of 385, 374, and 406 days, respectively. Using a rule of thumb developed in 2-D burnup calculations for cross section updates, calculations were performed assuming one library (one updated set of ORIGEN-S cross sections) for each 100 days of burnup, i.e., four cross-section updates were performed for each operational cycle.

Unfortunately, this approach proved to be inadequate for 3-D calculations, due to the broad variation in flux between centerline and the axial end region of the assembly. The power distribution amongst mixtures is calculated at each burnup step based on the composition in each mixture. The relatively coarse (in time) power updates resulted in instability in the predicted power profile, presumably to xenon and other fission product poisoning effects. The instability caused the power profile to oscillate between end and center regions of the core.

In retrospect, this behavior should have been expected, as it is a known issue in full-core modelling. Nevertheless, it was a departure from experience gained in two-dimensional analysis. Numerical experimentation found that the power oscillations could be eliminated by increasing the frequency of power updates, especially early in life. Additional temporal discretization could have been used, however, the nature of the Monte Carlo solution mandated using as few time steps as was practical to complete calculations in an acceptable time period of less than one week. Hence, the burnup history shown in Table 1 was applied in all subsequent calculations.

Table 1.
Depletion model for SF97-1 fuel sample.

Power (MW/tonne)	Burn time (d)	Down time (d)	No. of updates
14.76	385	88	15
15.74	374	6	11
13.97	406	1446	14

2.3. Axial reflection

Initially, due to lack of detailed assembly design information, a 30 cm water region was assumed beyond the end of the fuel rod. After completing the initial study, it was realized that the assumption of 30 cm of water was potentially a significant contributor to the end-of-fuel behaviour, so a second set of calculations was performed in which a homogeneous mixture of equal volumes of water and stainless steel was assumed This was thought to provide an upper bound on steel content, and was used to assess the impact of the assumed boundary condition on axial depletion.

2.4. Fuel sample location

The first set of calculations was performed with the assayed sample placed in the first (endmost) 0.9cm segment based on reported postion. As discussed below, results showed poor spectral agreement with measured data, and additional calculations were performed assuming the sample was located in each of the remaining six pellet-sized axial segments of 0.9-cm height. For each calculation, the burnup history of Table 1 was applied to the region assumed for the sample. Isotopic concentrations were extracted for each of the seven axial cells and converted to units of mg per initial gram of uranium, consistent with reported measurement results.

2.5. Variations in sample location

Initial calculations for the first pellet location, corresponding to the estimated 0.4cm at the top (measured from the end of the fuel stack) of the fuel rod, showed very poor prediction of all nuclides, especially the plutonium nuclides, for both boundary condition approaches. This suggested that the spectrum within the last pellet was significantly softer than that of the measured sample. However, it was also recognized that there was some uncertainty associated with the measured location of the sample. The size of the top end plug was assumed to be 2.0 cm due to lack of actual data. Additionally, it is not clear if plenum size specifications reflected the as-built dimensions, or if axial fuel swelling was accounted for in the provided fuel dimensions. Finally, information on structural materials located beyond the fuel end plugs is not available.

3. Results

As discussed earlier, calculations were performed in 0.9 cm (pellet-sized) increments, assuming that the sample was extracted from one of the pellets near the end, if not the very last one. It is believed that the error in location was likely not more than two cm, hence the sample was most likely taken from one of the bottom three pellets; however, calculations were performed assuming the sample was taken from each of the seven end pellets, in order to establish trends as a function of distance from the end of the rod. Tables 2 and 3 show the results of the calculations for selected nuclides for which measurement data were available. Results are reported in terms of the ratio of calculated to experimental concentrations (C/E) for each pellet location for the models based on the water boundary condition and the water/steel boundary condition, respectively.

The last two rows of the tables show the average of the C/E ratios for all nuclides, and for actinides only. In general, radiochemical measurements for actinides have less uncertainty than those for fission products (see Table 4); additionally, C/E ratios for actinides are generally closer to 1.0, on average, than those for fission products, believed to be due to better available data for actinides (Sanders and Gauld, 2003). Neither is seen as an absolute indicator of best agreement, but both are reported to better understand behaviors and trends.

The results corresponding to each boundary condition type, water only and water-steel, are discussed in the following subsections.

3.1. Water-only reflection

The results of Table 2 indicate that pellet location 3, which is 1.8 to 2.7 cm from the top of the active fuel region, provides the best agreement with measured data. Pellet locations 1 and 2 show a significant under-prediction of plutonium nuclides – these nuclides are much better predicted in the pellet 3 location. Note that moving further from the end of the rod results in over-prediction of plutonium nuclides coming from spectral hardening. The final column of Table 2 provides C/E ratios computed using a 2-D approximation in KENO-VI, i.e., a model with uniform fuel axially and reflective boundary conditions.

3.2. Mixed water-steel reflection

Based on the results given in Table 3, pellet location 5, which is located approximately 3.6 – 4.5 cm from the end of the rod, is most consistent with the measured data. The average actinide and plutonium isotopes appear to be best predicted at this location. Nd-148 and Cs-137, which are generally excellent burnup indicators, would also tend to support this conclusion as both are maximized (but not quite unity) in this vicinity.

In general, the same trends are observed in both model types. As discussed earlier, it is thought that the error in the location of the sample is no more than 2 cm. Measurement error that would have taken the sample from the fifth pellet from the top is unlikely. This suggests that the water-steel boundary condition is a significant departure from the physical configuration of the in-reactor assembly. On the other hand, this behavior may also indicate that the water-only axial boundary condition is not an extreme approximation.

Table 2.
Calculated to experimental (C/E) nuclide number density ratios for sample SF97-1, water-only axial reflection.

Nuclide	3D Calculations							2D Calcs.
	Pellet 1 (0-0.9cm)	Pellet 2 (0.9-1.8cm)	Pellet 3 (1.8-2.7cm)	Pellet 4 (2.7-3.6cm)	Pellet 5 (3.6-4.5cm)	Pellet 6 (4.5-5.4cm)	Pellet 7 (5.4-6.3cm)	
U-234	1.171	1.116	1.089	1.046	1.073	1.107	1.020	1.067
U-235	1.000	1.023	1.043	1.068	1.047	1.112	1.051	1.031
U-236	0.993	0.893	0.948	0.932	0.976	0.892	0.906	0.942
U-238	1.042	1.032	0.958	0.962	1.003	0.990	1.022	0.985
Np-237	0.654	0.843	0.973	1.130	1.071	1.101	1.208	1.191
Pu-238	0.557	0.784	0.863	1.056	1.155	1.129	1.215	1.231
Pu-239	0.778	0.965	1.064	1.173	1.271	1.308	1.316	1.310
Pu-240	0.914	0.975	1.011	1.145	1.088	1.180	1.125	1.109
Pu-241	0.661	0.774	0.982	1.165	1.169	1.239	1.344	1.308
Pu-242	0.746	0.877	0.936	1.086	1.102	1.195	1.158	1.203
Am-241	0.782	1.088	1.291	1.455	1.470	1.626	1.739	1.717
Cm-242	0.569	0.697	0.826	1.038	1.027	1.090	1.158	1.646
Cm-244	0.382	0.617	0.927	1.363	1.447	1.675	1.974	1.091
Nd-143	0.943	1.000	0.969	1.001	1.017	0.981	1.020	1.843
Nd-144	1.102	1.084	0.998	0.992	1.040	0.979	0.959	1.024
Nd-145	0.991	1.033	0.977	1.033	1.004	1.020	1.004	1.042
Nd-146	1.044	1.031	1.034	0.986	0.956	0.994	0.971	0.950
Nd-148	1.014	0.954	0.949	1.028	1.021	1.035	0.965	0.999
Nd-150	0.962	0.997	1.011	1.060	1.029	0.978	1.019	1.005
Cs-137	0.959	0.935	1.000	0.920	0.988	0.958	0.979	0.967
Cs-134	0.640	0.694	0.773	0.889	0.866	0.879	0.928	0.910
Eu-154	0.701	0.775	0.967	1.124	1.088	1.140	1.221	0.953
Sb-125	1.206	1.160	1.201	1.331	1.273	1.305	1.255	1.186
Ru-106	0.756	0.799	0.841	0.888	0.931	0.910	0.966	1.255
Average	0.857	0.923	0.985	1.078	1.088	1.118	1.147	1.165
Actinide Average	0.788	0.899	0.993	1.125	1.146	1.203	1.249	1.218

Table 3
Calculated to experimental (C/E) nuclide number density ratios for SF97-1, 50/50 water-steel axial reflection

Nuclide	3D calculations							2D calcs.
	Pellet 1 (0-0.9cm)	Pellet 2 (0.9-1.8cm)	Pellet 3 (1.8-2.7cm)	Pellet 4 (2.7-3.6cm)	Pellet 5 (3.6-4.5cm)	Pellet 6 (4.5-5.4cm)	Pellet 7 (5.4-6.3cm)	
U-234	1.078	1.028	1.003	0.963	0.988	1.019	0.939	1.067
U-235	0.921	0.942	0.960	0.983	0.964	1.024	0.968	1.031
U-236	0.914	0.822	0.873	0.858	0.899	0.821	0.834	0.942
U-238	0.959	0.950	0.882	0.886	0.924	0.912	0.941	0.985
Np-237	0.602	0.776	0.896	1.040	0.986	1.014	1.112	1.191
Pu-238	0.513	0.722	0.795	0.972	1.063	1.040	1.119	1.231
Pu-239	0.716	0.889	0.980	1.080	1.170	1.204	1.212	1.310
Pu-240	0.842	0.898	0.931	1.054	1.002	1.086	1.036	1.109
Pu-241	0.609	0.713	0.904	1.073	1.076	1.141	1.237	1.308
Pu-242	0.687	0.808	0.862	1.000	1.015	1.100	1.066	1.203
Am-241	0.720	1.002	1.189	1.340	1.354	1.497	1.601	1.717
Cm-242	0.524	0.642	0.761	0.956	0.946	1.004	1.066	1.646
Cm-244	0.352	0.568	0.854	1.255	1.332	1.542	1.818	1.091
Nd-143	0.939	1.025	0.951	0.988	0.982	0.964	1.037	1.859
Nd-144	1.133	1.073	1.018	0.958	1.011	1.020	0.996	0.990
Nd-145	1.025	1.049	1.013	1.029	0.969	1.053	0.990	1.049
Nd-146	1.013	1.065	1.040	1.007	0.924	1.019	0.973	0.979
Nd-148	0.974	0.976	0.938	1.055	1.058	1.010	0.961	1.038
Nd-150	0.945	1.038	0.987	1.099	0.992	1.004	1.002	0.981
Cs-137	0.952	0.922	0.974	0.897	1.019	0.954	0.970	0.970
Cs-134	0.699	0.682	0.711	0.815	0.887	0.910	0.851	0.973
Eu-154	0.645	0.714	0.890	1.035	1.002	1.050	1.124	0.953
Sb-125	1.110	1.068	1.106	1.226	1.172	1.202	1.156	1.186
Ru-106	0.696	0.736	0.774	0.818	0.857	0.838	0.889	1.255
Average	0.695	0.722	0.767	0.808	0.863	0.867	0.915	1.165
Actinide Average	0.785	0.845	0.901	0.985	0.996	1.023	1.050	1.218

3.3. Spectral analysis

Each KENO-VI calculation provides spectral information in terms of fluxes by energy group. Figure 2 shows the neutron spectrum calculated in each fuel pellet, compared to the 2-D spectrum that would characterize a sample located farther from the axial end of a rod, for the water-only-boundary model. There is a clear increase in the fast neutron population as calculations move farther from the top end of the fuel; however, even pellet 7, centered 5.9cm from the top of the rod, shows a reduced fast neutron component relative to the 2-D model.

Note that the uncertainties on the fluxes are considerably larger for each of the seven pellet locations relative to the 2-D model. This is due to the nature of the Monte Carlo calculation itself – neutrons densities are dominant in the most reactive regions of the core; in a 3-D calculation, the axial end of the fuel rod is less well represented relative to the center of the rod. In a 2-D calculation, there is no axial variation and sampling uncertainty is significantly reduced.

Table 4.
Analytical measurement uncertainties for nuclide measurements (Sanders and Gauld, 2003)

Isotope	Measurement Uncertainty
U-234	< 1%
U-235, -238	< 0.1%
U-236	< 2%
Pu-238	< 0.5%
Pu-239, -240, -241, -242	< 0.3%
Nd, Sm isotopes	< 0.1%
Am-241, Cm-244	< 2%
Cm-242	< 10%
Gd isotopes	< 0.1%
Np-237	< 10%
Cs-134, Cs-137, Eu-154	< 3%
Ru-106	< 5%
Sb-125	< 10%

4. Conclusions

Results indicate that uncertainties in the placement of the SF97-1 fuel sample render this measurement of limited value in the validation of 3-D depletion calculations. The results presented indicate that the location of the sample was perhaps an additional 1.5 to 2.5 cm from the top of the rod than reported. Additionally, the structure of the assembly and fittings beyond the end of the fuel will have some effect on the model, and this information is not readily available in the original report of measured data. Clearly, the 3-D leakage effects render this sample inappropriate for 2-D calculations. Further calculations are needed to determine the effect of varying the moderator/steel ratio beyond the end of the fuel rod, and to determine how far into the length of the fuel rod is influenced by axial leakage.

Another issue that was not accounted for was the influence of adjacent assemblies. In a 3-D model, burnup of the central region of the fuel assembly will result in a shift in the peak flux toward the ends of the assembly. Although such behavior is observed in fuel assemblies within a single fuel cycle, core reload with fresh fuel assemblies will move core flux peaks back toward the axial center of the core. In using a single assembly for all depletion calculations, axial flux would move toward the ends of the fuel throughout the depletion calculation. This may be a minor effect, but should be evaluated in future studies of 3-D depletion.

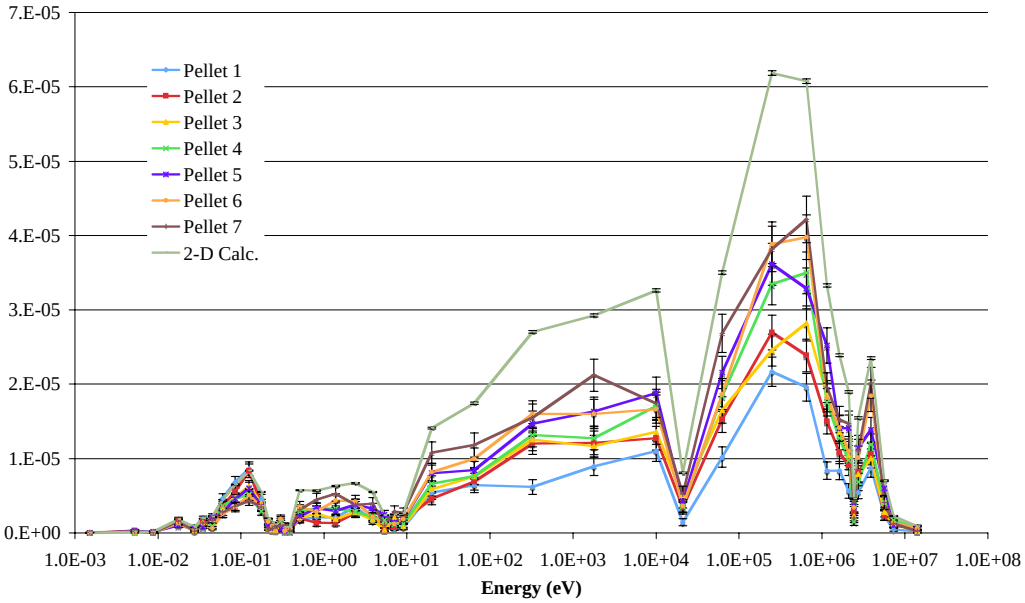

Fig. 2. Neutron spectrum as a function of position relative to the top of the SF97 fuel rod for water-only axial reflection.

Finally, there is some uncertainty associated with the assembly pitch applied in these calculations, since it was not supplied with the measurement data and was assumed based on similar designs. The sample rod was located on the assembly periphery, hence the influence of inter-assembly moderator would be important. However, this effect is probably washed out by the uncertainty in the axial configuration beyond the end of the fuel rods.

Based on the observations noted herein, it is reasonable to conclude that RCA measurements near the axial ends of a fuel sample provide little value in terms of validation for 2D depletion methods. And while measurements near the end of a fuel rod do provide some value for 3D depletion methods, care must be taking in determination of the precise location of the fuel sample, and additional information on the assembly and core structural design in the vicinity of the sample is extremely important.

TRITON's T5-DEPL and T6-DEPL sequences, based on the Monte Carlo codes KENO V.a and KENO-VI, respectively, have been validated in the past for a number of effectively 2-D radiochemical assay measurements, and by comparison to the 2-D deterministic T-DEPL sequence (DeHart and Bowman, 2005). Although this 3-D measurement for sample SF97-1 does not serve to validate T6-DEPL due to uncertainties in the measurement itself, it does appear to demonstrate the ability of the T6-DEPL sequence to capture 3-D effects. Issues associated with Monte Carlo depletion (propagation of uncertainties and variance reduction) remain to be addressed. However, in this case the spectral effects of spatial positioning appear to outweigh the effect of stochastic uncertainty, and a spectral shift with position is clearly seen.

References

Brady, M. C., Parks, C. V., and Marotta, C. R.. 1990, End effects in the criticality analysis of burnup credit casks, Trans. Am. Nucl. Soc. 62, 317.

DeHart, M. D., 1996, Sensitivity and Parametric Evaluations of Significant Aspects of Burnup Credit for PWR Spent Fuel Packages, ORNL/TM-12973, Lockheed Martin Energy Research Corp., Oak Ridge Natl. Lab.

DeHart, M. D., 1999, Parametric analysis of PWR spent fuel depletion parameters for long-term disposal criticality safety, ORNL/TM-1999/99, Lockheed Martin Energy Research Corp., Oak Ridge Natl. Lab.

DeHart, M. D. and Bowman, S. M., 2005, Improved radiochemical assay analyses using TRITON depletion sequences in SCALE, Proceedings of the IAEA technical committee meeting on advances in applications of burnup credit to enhance spent fuel transportation, International Atomic Energy Agency Technical Committee Meeting, London, U.K.

Haeck, W. and Verboomen, B., 2007, An optimal approach to Monte Carlo burn-up, Nucl. Sci. Eng., 156, 180-196

Mochizuki, H., Suyama, K. and Okuno, H, 2003, "SWAT2: the improved SWAT code system by incorporating the continuous energy monte carlo code MVP" International Conference on Nuclear Criticality - ICNC'2003, Tokaimura, Japan.

Nakahara, T., Suyama, K., and Suzaki, T., eds., 2000, Technical development on burnup-credit for spent LWR fuels, JAERI-Tech 2000-071, Japan Atomic Energy Research Institute (JAERI), Tokai-mura, Naka-gun, Ibaraki-ken, Japan, October 2000. [ORNL/TR-2001/01 English Translation, Oak Ridge National Laboratory, January 2002.]

Nouri, A., 1998, OECD/NEA burnup credit criticality benchmark - analysis of Phase II-B results: conceptual PWR spent fuel transportation cask, IPSN/98-05 (NEA/NSC/ DOC(98)1), Institut de Protection et de Surete Nucleaire.

Poston, D. L. and Trellue, H. R., 1999, User's manual, version 2.0 for MONTEBURNS version 1.0," LA-UR-99-4999.

Sanders, C. E. and Gauld, I. C., 2003, Isotopic analysis of high-burnup PWR spent fuel samples from the Takahama-3 reactor, NUREG/CR-6798 (ORNL/TM-2001/259), UT-Battelle, LLC, Oak Ridge National Laboratory.

Turner, S. E, 1989, An uncertainty analysis – axial burnup distribution effects, Proc. Workshop Use of Burnup Credit in Spent Fuel Transport

Casks, Washington D.C., February 21-22, 1988, SAND89-0018, TTC-0884, UC-820, T. L. Sanders, Ed., Sandia National Laboratories

Wagner, J.C. and DeHart, M. D., 2000, Review of axial burnup distribution considerations for burnup credit calculations, ORNL/TM-1999/246, Lockheed Martin Energy Research Corp., Oak Ridge Natl. Lab.